

Mono-X signal and two component dark matter: new distinction criteria

Subhaditya Bhattacharya,^{1,*} Purusottam Ghosh,^{2,†} Jayita Lahiri,^{1,‡} and Biswarup Mukhopadhyaya^{3,§}

¹*Department of Physics, Indian Institute of Technology Guwahati, Assam-781039, India*

²*School Of Physical Sciences, Indian Association for the Cultivation of Science,
2A and 2B, Raja S.C. Mullick Road, Kolkata 700032, India*

³*Department of Physical Sciences, Indian Institute of Science Education and Research Kolkata, Mohanpur - 741246, India*

The identification and isolation of two WIMP dark matter (DM) components at colliders is of wide interest on the one hand but extremely challenging on the other, especially when the dominant signal of both DM components is of the mono-X type ($X = \gamma, Z, H$). After emphasizing that an e^+e^- collider is more suitable for this goal, we first identify the theoretical principles that govern the occurrence of two peaks in missing energy (\cancel{E}) distribution, in a double-DM scenario. We then identify a variable that rather spectacularly elicits the double-peaking behaviour, namely, the plot of bin-wise statistical significance (S/\sqrt{B}) against \cancel{E} . Using Gaussian fits of the histograms, we apply a set of criteria developed by us, to illustrate the above points numerically for suitable benchmarks.

More than one weakly interacting massive particles (WIMP) as DM components are quite viable [1–6]. They should in general lead to missing energy (\cancel{E}) or missing transverse energy (E_T) at colliders. However, distinguishing, say, two DM components in collider experiments is rather challenging in general, and are possible under certain circumstances only. The task is especially arduous if the major collider signal consists in mono-X plus \cancel{E} (with $X = \gamma, Z, h$), primarily due to the very limited number of kinematic variables at our disposal, and partially due to the apparent insurmountability of Standard Model (SM) backgrounds. The present work is aimed at meeting such challenges.

e^+e^- colliders may be better suited for isolating two WIMP DM particles if they are kinematically accessible. This is mainly due to (a) the possibility of using \cancel{E} as a variable, which depends on DM mass, (b) availability of missing longitudinal momentum as a source of extra information, (c) less SM background contamination, and (d) the advantage of initial beam polarisation [7, 8]. The rest of the discussion is therefore in the context of e^+e^- machines. We illustrate the criteria for double-DM signals being identifiable in e^+e^- colliders, using some phenomenologically selected benchmarks. In particular, we suggest a variable that rather spectacularly enables the distinction between the two DM components, namely, the bin-wise signal significance in the missing-energy distribution.

Challenge 1: Will there always be noticeable peaks/bumps? Mono-X signals are generic to any WIMP model, which result from direct production of a DM pair (when the DM is stabilised by a symmetry such as Z_2) typically in absence of an extended dark sector [9–14]. It has the simplest event topology, and at the same time leaves one with limited choice in analysing the final state kinematics. Bumps in \cancel{E} distributions are driven by both kinematics and dynamics. Kinematics decide the minimum and maximum \cancel{E} for a given event, which in turn depend on the centre-of-mass (CM) energy and DM masses. Energy-momentum conservation plays an

important role here. On the other hand, the shape of the \cancel{E} distribution, both at the edges and in between, depends on the dynamics, namely, the Lagrangian, including possible sources of soft or collinear divergence.

Table I shows a set of effective (EFT) operators involving an iso-singlet DM (χ), stabilised by a Z_2 symmetry, interacting with SM particles which can lead to $e^+e^- \rightarrow \chi\chi X$ ($X = \gamma, Z, H$) [15–18]. This can happen via either $2 \rightarrow 3$ hard scattering, or through $2 \rightarrow 2$ DM pair production along with radiation of a γ, Z or H from one of the legs. The benchmarks on which we base our illustrative numerical predictions include dual-DM scenarios with both scalars, fermions and combinations of them. Note further that the operators listed here are merely indicative, and by no means constitute an exhaustive list. However, whether the bump-hunting approach works for a particular operator depends on the following principles:

DM-type	Name	Operator
Scalar	O_1^s	$\frac{1}{\Lambda^2} \bar{L}(\Phi \ell_R)(\chi^2)$
Scalar	O_2^s	$\frac{1}{\Lambda^4} (\bar{L} D_\mu \Phi \ell_R)(\chi \partial_\mu \chi)$
Scalar	O_3^s	$\frac{1}{\Lambda^2} (B_{\mu\nu} B^{\mu\nu} + W_{\mu\nu} W^{\mu\nu})(\chi^2)$
Fermion	O_1^f	$\frac{1}{\Lambda^2} (\bar{L} \gamma^\mu L + \bar{\ell}_R \gamma^\mu \ell_R)(\bar{\chi} \gamma_\mu \chi)$
Fermion	O_2^f	$\frac{1}{\Lambda^3} (\bar{L} \Phi \ell_R)(\bar{\chi} \chi)$
Fermion	O_3^f	$\frac{1}{\Lambda^3} (B_{\mu\nu} B^{\mu\nu} + W_{\mu\nu} W^{\mu\nu})(\bar{\chi} \chi)$

TABLE I. Samples of DM-SM EFT operators involving iso-singlet DM (χ) as scalar or fermion. $B_{\mu\nu}$ and $W_{\mu\nu}$ are electroweak field strength tensors, $L(\ell_R)$ are left (right)-handed SM lepton doublet (singlet), Φ is the SM Higgs doublet, D_μ is the gauge-covariant derivative and Λ is the cut-off scale of the EFT operators.

1. Angular momentum conservation: This is often related to the chiral structure of the interactions involved. There can be situations where a particular spatial configuration and the relative directionality of the particles is not allowed by the angular

momentum conservation, given the helicity assignments demanded by the underlying interactions. In that case we see a drop in the differential distribution in $\frac{d\sigma}{d\cancel{E}}$ or zeroes at the edge(s) of the phase space, providing a peaking behaviour.

2. Rotational invariance in Minkowski space ($E^2 - |p|^2 = m^2$): The last integrand before arriving at the differential distribution such as $\frac{d\sigma}{d\cancel{E}}$, always contains a positive power of the of three-momentum of a final state particle. Therefore the final state particles being at rest automatically causes the differential distribution to vanish resulting a peak-like behaviour, unless the drop is assuaged by a factor in the denominator, where the same three-momentum occurs.
3. Collinear divergence: Arises when the radiated γ is collinear to the initial or final state particles and dominantly controls features of the distributions. A massive propagator which does not lead to collinear divergence, may still lead, instead of a drop, to a rise at an edge of the phase space due to a three momentum factor in the denominator. A soft photon corresponding to the maximum of \cancel{E} , accompanied by an infrared divergence, may also cause such a rise.
4. Operator structure: The exact position of the maxima of the distributions are often dictated by the specific interaction in question.

Our study is centred around double bump hunting in \cancel{E} distributions coming from two DM components. In Figure 1 we show two examples of \cancel{E} distributions in mono- γ signal, where double peak behaviour is observed, when two DM particles from two different operators are pair-produced in e^+e^- collision at $\sqrt{s} = 1$ TeV. Figure 1(top) shows mono- γ contributions coming from O_3^s and O_2^f . The peaking behaviour around the minimum of \cancel{E} is obtained because (i) there is no collinear divergence at this kinematic point, and (ii) this region is not disfavoured by angular momentum conservation, thanks to the chiral structure of the interaction responsible for this peak (O_3^s). O_3^s provides a photon mediated final state consisting of a photon and two scalar DMs. The resultant spin one state corresponds to the minimum \cancel{E} configuration when the photon moves oppositely to the two DM particles. The rise at the maximum of \cancel{E} , on the other hand, is because of collinear as well as infrared divergence, since the γ emitted is not only rather soft but also at a small angle with the initial e^\pm , something that in this case is not disfavoured by angular momentum conservation. The same features control the rise in maximum \cancel{E} in bottom panel of Figure 1, where contributions from O_3^f and O_2^f are shown. At the minimum of

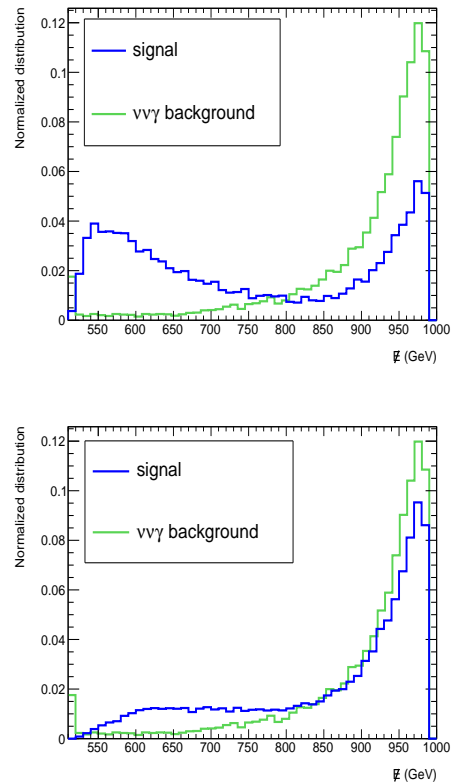


FIG. 1. Normalised \cancel{E} distribution in the mono- γ final state for two DM components arising from (top) O_3^s and O_2^f and (bottom) O_3^f and O_2^f operators, for DM masses 100 GeV and 200 GeV respectively, together with $\nu\bar{\nu}\gamma$ background. We choose $\sqrt{s} = 1$ TeV, $\Lambda = 1.2$ TeV with $P_{e^+} = +30\%$, $P_{e^-} = +80\%$.

\cancel{E} , however, there is a suppression demanded by angular momentum conservation in operator O_3^f , and that is why the peaking behaviour is relatively indistinct. The SM background distributions are also shown; we shall shortly come back to the strategy on backgrounds for all mono-X events.

We note here that the double peaking behaviour can also arise from a single DM component, when DM is nearly massless compared to \sqrt{s} , since a collinear divergence can then occur even at the minimum of \cancel{E} . On the other hand, the combined $\frac{d\sigma}{d\cancel{E}}$ distributions for two DM particles from two different operators can provide a single peak, when the individual distributions are identical and shows a collinear shoot-up at the maximum \cancel{E} and a suppression at the minimum \cancel{E} due to the structure of relevant operators. This is avoidable if one of the two mono- γ generating processes is driven by an effective interaction vertex as chosen above, as opposed to the case where the photon is emitted via bremsstrahlung.

Next, we take up the mono- Z and mono- H signals, illustrative predictions for which are shown in Figure 2.

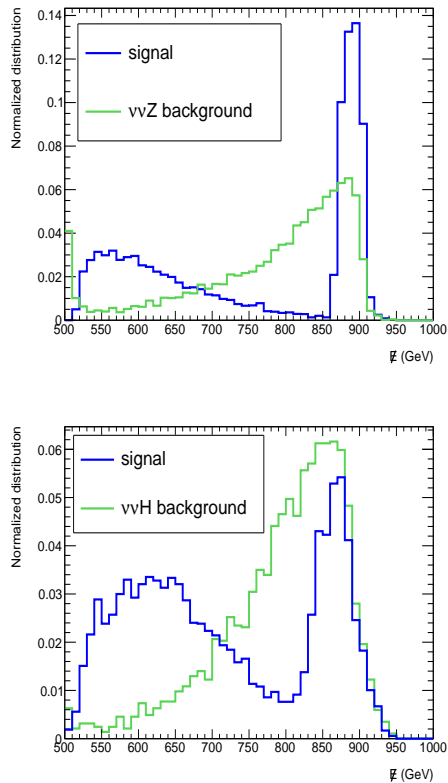


FIG. 2. Normalised \cancel{E} distribution for (top) mono- Z final state for two DM components arising from O_3^s and O_1^f , (bottom) mono- H final state for two DM components from O_2^s and O_1^s , with masses 100 GeV and 400 GeV respectively. SM backgrounds are also shown. We choose $\sqrt{s} = 1$ TeV, $\Lambda = 1.2$ TeV and $P_{e^+} = +30\%$, $P_{e^-} = +80\%$.

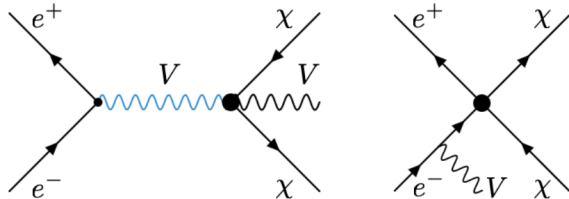


FIG. 3. Feynman graphs contributing to mono- V ($V = \gamma, Z$) events in this analysis.

O_3^s and O_1^f are considered for mono- Z (top panel), O_2^s and O_1^s for mono- H (bottom panel) with details of the parameters stated in the caption. We have reconstructed the mono- Z and mono- H events in the $\ell^+\ell^-$ ($\ell = e, \mu$) and $b\bar{b}$ channel, respectively, with the standard trigger and selection cuts. For both the plots in Figure 2, the distribution is brought down to zero for maximum \cancel{E} . The reason behind this being the occurrence of $(E^2 - m^2)$ in the numerator of the penultimate integrand in cross-

section calculation. This factor, traceable to rotational invariance in the Minkowski space, causes the distribution to vanish at the maximum of \cancel{E} , which corresponds to zero three-momentum of the Z or the H . This is conducive to peaking behaviour corresponding to each of the two DM components, so long as the behaviour of low \cancel{E} is favoured by angular momentum conservation, especially since there is now no collinear divergence at the higher end. One may thus see two peaks, the level of shift to the left for each peak being governed by the corresponding DM mass; their splitting thus becomes the deciding factor in the isolation of the peaks. An exceptional case is the operator O_1^f where the Z can be emitted via bremsstrahlung, for which the peak occurs at the higher end of \cancel{E} spectrum for any DM mass due to the appearance of a small number $\sim m_Z^2/s$ in the denominator of the penultimate integrand. Feynman graphs that contribute to mono- V events ($V = \gamma, Z$) considered in this analysis are shown in Figure. 3, that are typical to result double bump in \cancel{E} distributions.

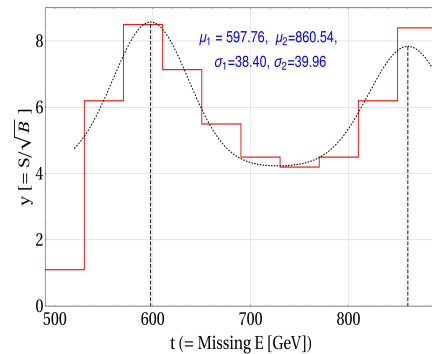


FIG. 4. Variation of local signal significance and Gaussian fitting as a function of \cancel{E} in the mono- γ signal as in Fig. 1(bottom) at 100 fb^{-1} luminosity. Global signal significance = 5σ and $S/B \approx 4\%$.

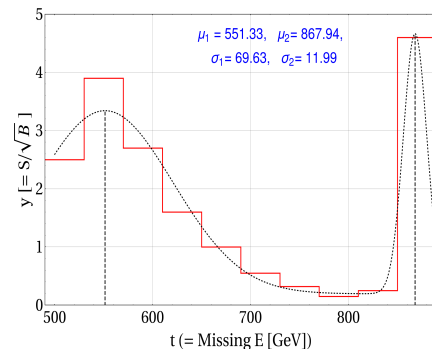


FIG. 5. Variation of local signal significance and Gaussian fitting as a function of \cancel{E} for mono- Z signal as in Figure 2(top) at 1000 fb^{-1} luminosity. Global signal significance = 4.7σ and $S/B \approx 5\%$.

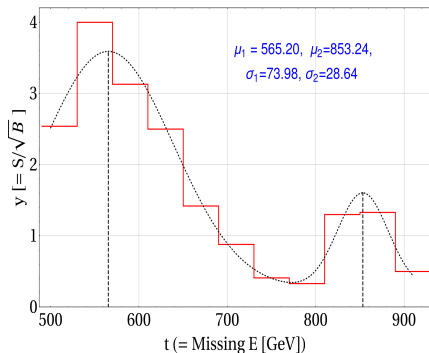


FIG. 6. Variation of local signal significance and Gaussian fitting as a function of \cancel{E} for mono- H signal as in Figure 2(bottom) at 3000 fb^{-1} luminosity. Global signal significance = 4.2σ and $S/B \approx 4\%$.

We have used MADGRAPH[19] in tandem with DELPHES with the ILD card [20], as a result of which the behaviour seen in the distributions deviate a little bit from the usual ones. Specific beam polarisation ($P_{e^+} = +30\%$, $P_{e^-} = +80\%$) choices are made to optimise the relative heights of both the peaks.

Challenge 2: How to make the double peaks rise above the backgrounds? We have seen above some examples of cases where two peaks/bumps corresponding to the two DM particles are noticeable. However, it is not obvious that the peaks are distinct when different kinds of $\nu\bar{\nu}X$ ($X = \gamma, Z, H$) backgrounds as already shown in Figs. 1 and 2, are taken into account. While we consider all possible backgrounds, the most menacing ones that tend to drown the mono- Z and mono- H signals is the one from vector boson fusion (VBF). There are, after all, not too many kinematic variables at our disposal in this case. How then can one rise above the irreducible backgrounds?

Two generic criteria for this to happen, securing the best signal-to background ratio, are: (i) The signal peak that is closest to the SM background peak should rise as much above the latter as possible, and (ii) the other signal peak, after any distortion by the background, should still be as distinct from the first one as is possible.

In order to make the double peak distinct in spite of backgrounds, we propose a new observable here. This is the bin-by-bin signal significance S/\sqrt{B} for an integrated luminosity optimised for different DM benchmarks. This ‘local significance’, plotted against \cancel{E} , is shown in Figures 4, 5, 6 for the three types of mono- X signals. We present alongside the Gaussian fits of the corresponding histograms, using :

$$\begin{aligned} G(x) &= G_1(x) + G_2(x) + \mathcal{B} \\ &= A_1 e^{-\frac{(x-\mu_1)^2}{2\sigma_1^2}} + A_2 e^{-\frac{(x-\mu_2)^2}{2\sigma_2^2}} + \mathcal{B}. \end{aligned} \quad (1)$$

The values of μ_1 , μ_2 , σ_1 and σ_2 in each case are indicated

in the figure insets. In the examples shown here, we have taken the bin size along the \cancel{E} -axis to be 40 GeV, which in most of cases optimise the significance. The central outcome of this is a rather remarkable distinctiveness of the two DM peaks, as evinced from all the three Figs. 4, 5, 6. The global significance and the overall S/B are given in the corresponding figure captions; one can notice S/B ratios ranging upto 10%, and the global significance ranging between $4 - 5\sigma$. This not only assures one of the usefulness of the suggested distributions but also indicates the level of refinement required in an e^+e^- experiment in connection with the reduction of systematic errors.

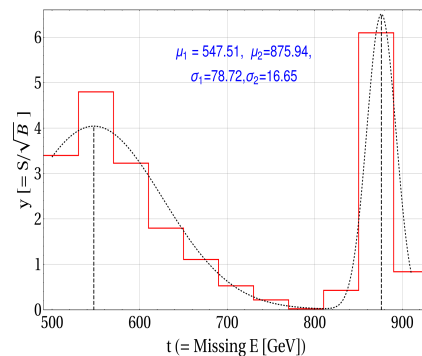


FIG. 7. Same as Figure 5, after applying the cut $E_T < 50$ GeV or > 200 GeV at 1000 fb^{-1} luminosity. This amounts to $S/B \approx 16\%$ and a global significance 7σ .

While the local significance plots turn out to be decidedly helpful for all three types of mono- X signals, we would especially like to draw the reader’s attention to Figure 4, where monophoton events are considered. If one compares it with the Figure 1(bottom), one finds the double-peak feature rather smudged out. In Figure 4 however, the double peaks show up much more prominently in terms of the bin-by-bin significance, demonstrating the efficacy of this variable.

Is there any way of further improving the discernibility of the two peaks? In response to this query, we suggest further application of an E_T -cut on the signal and the backgrounds. Since E_T and \cancel{E} are *correlated only partially*, and the DM mass enters into \cancel{E} manifestly, one can, with judicious E_T cuts, make the two peaks more distinct, and at the same time improve the global significance and the signal-to-background ratio. This is illustrated in Figure 7. It should be remembered, though, that the E_T -cuts need to be customised after noticing the double-peak appearance first, lest one could either slice through the middle on a single peak and lead to fake double-peak events or reduce the height of one of the peaks in an actual double-peak event so that it effectively looks like a single peak.

The next question is: how to quantify the distinguishability of the two peaks in a mono- X signal? For this pur-

pose we refer the reader to reference [21] where, in the context of the double-peak events generated in cascades, a number of distinction criteria $C_i (i = 1 - 4)$ have been developed; leading to the quantities $R_{C_i} (i = 1 - 4)$. The variables R_{C_3} , R_{C_4} emerge as the most useful ones, although the others, too, have varying degrees of efficacy for different benchmarks. As discussed in [21], R_{C_3} reflects a comparative estimate of the number of events in the vicinity of the two peaks, and smaller R_{C_3} implies that the second peak is more significant relative to the first one. R_{C_4} quantifies the presence of the peaks with respect to the minimum in between, and its bigger values indicate better distinguishability. In Table II, we present the values corresponding to our chosen benchmark points, based on Gaussian fits of the significance histograms. We note further that for the chosen benchmarks, (a) Mono- γ requires the least integrated luminosity, (b) Mono- Z leads to the best distinguishability in terms of peak separation, and (c) Mono- H requires the maximum integrated luminosity. The improvement brought about by the E_T is also visible.

Benchmarks in	R_{C_3}	R_{C_4}
Figure 4	4	1.8
Figure 5	16	10.1
Figure 6	38	2.1
Figure 7	23	38.5

TABLE II. The values of R_{C_3} and R_{C_4} for the chosen benchmarks, already discussed in Figures 4-7.

In conclusion, mono-X events in an e^+e^- collider bring in a big challenge in distinguishing between two DM components. This is in contrast to DM signals produced in cascades, where not only are backgrounds easier to reduce, but the occurrence of two peaks is also a more widespread phenomenon, as has been demonstrated in [21]. Our analysis of mono-X events identifies the physics underlying double-peak occurrence; we also demonstrate that bin-by-bin distributions in signal significance plotted against \cancel{E}_T obviates the double-peaking behaviour which the backgrounds otherwise tend to obliterate. It is also found by us that judicious \cancel{E}_T cuts serve to enhance the prominence of the two peaks as well as overall significance and signal-to-background ratios. We shall discuss in a more detailed paper other issues such as the demands on our sample theoretical scenario brought about by issues such as relic density or direct searches [22].

Acknowledgments: SB acknowledges the grant CRG/2019/004078 from SERB, Govt. of India.

* Email:subhab@iitg.ac.in

- [†] Email:pghoshiitg@gmail.com
[‡] Email:jlahiri29@gmail.com
[§] Email:biswarup.mukho@gmail.com
- [1] Q.-H. Cao, E. Ma, J. Wudka, and C. P. Yuan, "Multipartite dark matter," [arXiv:0711.3881 \[hep-ph\]](#).
 - [2] S. Bhattacharya, A. Drozd, B. Grzadkowski, and J. Wudka, "Two-Component Dark Matter," *JHEP* **10** (2013) 158, [arXiv:1309.2986 \[hep-ph\]](#).
 - [3] J. Herrero-Garcia, A. Scaffidi, M. White, and A. G. Williams, "On the direct detection of multi-component dark matter: implications of the relic abundance," *JCAP* **1901** no. 01, (2019) 008, [arXiv:1809.06881 \[hep-ph\]](#).
 - [4] M. Aoki and T. Toma, "Boosted Self-interacting Dark Matter in a Multi-component Dark Matter Model," *JCAP* **10** (2018) 020, [arXiv:1806.09154 \[hep-ph\]](#).
 - [5] G. Belanger, A. Mjallal, and A. Pukhov, "Two dark matter candidates: The case of inert doublet and singlet scalars," *Phys. Rev. D* **105** no. 3, (2022) 035018, [arXiv:2108.08061 \[hep-ph\]](#).
 - [6] J. Hernandez-Sanchez, V. Keus, S. Moretti, and D. Sokolowska, "Complementary collider and astrophysical probes of multi-component Dark Matter," [arXiv:2202.10514 \[hep-ph\]](#).
 - [7] K. Fujii *et al.*, "The role of positron polarization for the initial 250 GeV stage of the International Linear Collider," [arXiv:1801.02840 \[hep-ph\]](#).
 - [8] M. Habermehl, M. Berggren, and J. List, "WIMP Dark Matter at the International Linear Collider," *Phys. Rev. D* **101** no. 7, (2020) 075053, [arXiv:2001.03011 \[hep-ex\]](#).
 - [9] N. F. Bell, J. B. Dent, A. J. Galea, T. D. Jacques, L. M. Krauss, and T. J. Weiler, "Searching for Dark Matter at the LHC with a Mono-Z," *Phys. Rev. D* **86** (2012) 096011, [arXiv:1209.0231 \[hep-ph\]](#).
 - [10] A. Berlin, T. Lin, and L.-T. Wang, "Mono-Higgs Detection of Dark Matter at the LHC," *JHEP* **06** (2014) 078, [arXiv:1402.7074 \[hep-ph\]](#).
 - [11] ATLAS Collaboration, E. Tolley, "Dark Matter searches with Mono-X signatures at the ATLAS experiment," *PoS DIS2016* (2016) 107.
 - [12] CMS Collaboration, A. M. Sirunyan *et al.*, "Search for new physics in the monophoton final state in proton-proton collisions at $\sqrt{s} = 13$ TeV," *JHEP* **10** (2017) 073, [arXiv:1706.03794 \[hep-ex\]](#).
 - [13] E. Bernreuther, J. Horak, T. Plehn, and A. Butter, "Actual Physics behind Mono-X," *SciPost Phys.* **5** no. 4, (2018) 034, [arXiv:1805.11637 \[hep-ph\]](#).
 - [14] S. Bottaro, D. Buttazzo, M. Costa, R. Franceschini, P. Panci, D. Redigolo, and L. Vittorio, "Closing the window on WIMP Dark Matter," *Eur. Phys. J. C* **82** no. 1, (2022) 31, [arXiv:2107.09688 \[hep-ph\]](#).
 - [15] P. J. Fox, R. Harnik, J. Kopp, and Y. Tsai, "LEP Shines Light on Dark Matter," *Phys. Rev. D* **84** (2011) 014028, [arXiv:1103.0240 \[hep-ph\]](#).
 - [16] Y. J. Chae and M. Perelstein, "Dark Matter Search at a Linear Collider: Effective Operator Approach," *JHEP* **05** (2013) 138, [arXiv:1211.4008 \[hep-ph\]](#).
 - [17] S. Kundu, A. Guha, P. K. Das, and P. S. B. Dev, "A model-independent analysis of leptophilic dark matter at future electron-positron colliders in the mono-photon and mono-Z channels," [arXiv:2110.06903 \[hep-ph\]](#).
 - [18] B. Barman, S. Bhattacharya, S. Girmohanta, and

- S. Jahedi, “Effective Leptophilic WIMPs at the e^+e^- collider,” *JHEP* **04** (2022) 146, [arXiv:2109.10936 \[hep-ph\]](#).
- [19] J. Alwall, M. Herquet, F. Maltoni, O. Mattelaer, and T. Stelzer, “MadGraph 5 : Going Beyond,” *JHEP* **06** (2011) 128, [arXiv:1106.0522 \[hep-ph\]](#).
- [20] **DELPHES 3** Collaboration, J. de Favereau, C. Delaere, P. Demin, A. Giammanco, V. Lemaître, A. Mertens, and M. Selvaggi, “DELPHES 3, A modular framework for fast simulation of a generic collider experiment,” *JHEP* **02** (2014) 057, [arXiv:1307.6346 \[hep-ex\]](#).
- [21] S. Bhattacharya, P. Ghosh, J. Lahiri, and B. Mukhopadhyaya, “Distinguishing two dark matter component particles at e^+e^- colliders,” [arXiv:2202.12097 \[hep-ph\]](#).
- [22] S. Bhattacharya, P. Ghosh, J. Lahiri, and B. Mukhopadhyaya, “Work in Progress,”.